

Article

Improved Kinetic Data Acquisition Using An Optically Accessible Catalytic Plate Reactor with Spatially-Resolved Measurement Techniques. Case of Study: CO₂ Methanation

Jose A. Hernandez Lalinde, Kevin Kofler, Xuejie Huang and Jan Kopyscinski * 

Department of Chemical Engineering, McGill University, 3610 University Street, Montreal, QC H3A 0C5, Canada; jose.hernandezlalinde@mail.mcgill.ca (J.A.H.L.); kevin.kofler@mail.mcgill.ca (K.K.); xuejie.huang@mail.mcgill.ca (X.H.)

* Correspondence: jan.kopyscinski@mcgill.ca; Tel.: +1-514-398-4276

Received: 12 January 2018; Accepted: 19 February 2018; Published: 21 February 2018

Abstract: Modelling and optimization of chemical reactors require a good understanding of the reactions mechanism with the corresponding kinetic description. Therefore, high quality kinetic data are needed, which can be challenging to obtain, especially for fast and highly exothermic reactions such as the CO₂ methanation. Traditionally, kinetic studies rely on measuring the exit gas composition (1 data point per species and experiment) using differential reactors with diluted catalyst beds and reactants to avoid temperature change. Therefore, an optically accessible catalytic channel reactor was designed, which allowed for the chance to gather spatially-resolved information on axial gas composition and catalyst surface temperature, specifically by means of a movable sampling capillary and shortwave infrared-thermography (SWIR), respectively. A catalyst coated plate was placed at the bottom of the channel, while a set of two quartz glass plates covers the top. In the current study 35 data points per gas species were collect for 1 experiment conducted under laminar flow conditions at 425 °C. Catalyst surface temperature determined via a SWIR camera was not influenced by polyatomic molecules partaking in the reaction and thus did not falsify the kinetic data. The catalyst mass distribution along the reactor axis was determined, enabling the development of a correct reactor model for kinetic parameter estimation and model discrimination.

Keywords: spatially-resolved measurement; CO₂ methanation; IR-thermography; Ni/Al₂O₃; kinetic measurements; catalytic plate reactor; catalyst mass distribution

1. Introduction

Traditionally, kinetic data of heterogeneous catalyzed reactions are collected with small laboratory packed bed reactors either with or without gas recirculation. They are usually operated as differential reactors (i.e., conversion <10%) measuring the exit-gas composition under conditions where transport resistances are negligible. Thus, intrinsic reaction rates can be obtained by determine the incremental change of the reactant or product molar flow rates for a known catalyst loading inside the reactor. Typically, the reactors hold a few milligrams up to several grams of catalyst with particle sizes in the micro- to millimeter scale. To avoid excessive temperature changes from the nature of exothermic or endothermic reactions, highly diluted gas mixtures (>90% inert gas), and diluted catalyst beds are used. In addition, a serious limitation of these systems is the necessity to reach a gas composition at the reactor exit that is sufficiently far away from chemical equilibrium. These conditions under which the kinetic data are collected may not be industrially relevant. Working under industrially-relevant conditions usually requires a continuous process using an integral reactor, which has significant

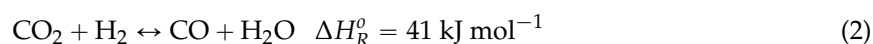
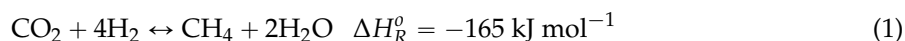
heterogeneities such non-uniform catalyst mass distribution, concentration and temperature gradients along the axial and radial directions. Kinetic measurements and modeling are difficult due to the lack of knowledge of these gradients [1]. For reactors without gas recirculation, each experiment results in a single data point per gas species. Therefore, combined kinetic parameter estimation and model discrimination of various proposed reaction mechanisms require a large number of experiments.

Operating the reactor as an integral reactor, while gathering information on gas composition and catalyst surface temperature as a function of the axial position in the reactor allows not only to minimize the number of experiments, but to investigate the reaction mechanism and kinetics in much more detail as it combines differential and integral reactor systems. Spatially-resolved measurement of gas composition and temperature can be determination by invasive and non-invasive techniques [2]. For example, direct sampling of the gas phase and temperature along the reactor axis can be achieved using a movable capillary and thermocouple or pyrometers, respectively, or via multiple fixed probing. These techniques have been applied in different reactor configurations such as monolith [3–5], coated metal foam [6–8], fixed bed [9] and fluidized bed [1]. The main disadvantage of the aforementioned setups is the unknown catalyst mass distribution along the reactor axis between the sampling points, thus they are not suitable for kinetic data collection.

Consequently, a catalytic plate reactor with the possibility to determine the spatial catalyst mass distribution has been developed and used to study the kinetics of syngas methanation and steam reforming [10,11]. This reactor combines spatially-resolved measurement of the gas composition profiles in the gas channel above the catalyst and its surface temperature by means of an open-ended movable sampling capillary and infrared (IR) thermography, respectively. The disadvantage of this setup is the use of an open-ended capillary that is supported on one side of the reactor only, which results in downward bending of the capillary. Thus, the capillary does not sample the gas composition at a constant height above the catalyst and in worst case the capillary might damage the catalyst surface.

IR thermography has advantages over inserted thermocouples, as thermocouples measure the gas temperature instead of the catalyst temperature, which can be significantly different especially for fast and strong exothermic reactions and leading to inaccurate kinetic data. Short- and Midwave-infrared cameras have been used to determine the catalyst surface temperature in various optically accessible reactors [10,12,13]. Shortwave infrared (SWIR) cameras are usually equipped with an indium gallium arsenide (InGaAs) sensor that can detect the radiation emitted from a hot surface in the 0.9 to 1.7 μm wavelength. However, thermography data can only be obtained at temperatures higher than 300 $^{\circ}\text{C}$. Midwave infrared (MIR) cameras, on the other hand, can determine the surface temperature down to 20 $^{\circ}\text{C}$ as they work in the 2 to 5 μm wavelength range. The disadvantages of MIR cameras are (1) the expensive cooled indium antimonide (InSb) detector, (2) the need for an expensive sapphire glass to be installed in the reactor and (3) the possibility that polyatomic molecules such as CO_2 , H_2O , and CH_4 adsorb the emitted infrared and thus falsify the temperature measurement. SWIR cameras are a cost-effective alternative that allows to use a standard quartz glass in the reactor design. In addition, polyatomic molecules should not influence the temperature measurements as they do not absorb radiation in the short wavelength range. However, this has not been proven for this kind of system [10,14].

This manuscript presents an optimized version of an optically accessible catalytic channel reactor allowing for simultaneous measurement of the catalyst surface temperature and gas composition profile under reaction conditions. This work includes details about reactor design considerations, catalyst coating, catalyst mass distribution, IR thermography and activity measurements for the CO_2 methanation over nickel containing ordered mesoporous alumina catalyst (OMA). The catalyzed CO_2 methanation is a fast and exothermic reaction and an important step in the Power-to-Gas process. In this process surplus electrical energy (i.e., wind energy) is converted into a grid compatible gas via water electrolysis to produce hydrogen and subsequent hydrogenation of captured carbon oxides to methane-rich gas [15,16]. The involved reactions (see Equations (1) and (2)) are catalyzed by supported Ni, Ru, and Rh systems, of which the latter two noble metals are more active [17–19]



Recently, new ordered mesoporous alumina catalysts (OMA) has shown great promise due to high specific surface areas, large pore volumes and uniform pore sizes compared to traditional catalyst systems [20], allowing for a better interaction between the metal-oxide and the support resulting a high metal dispersion.

2. Results and Discussion

2.1. Catalyst Coating and Catalyst Mass Distribution

An important aspect of the catalytic plate reactor is the catalyst washcoating and its characteristics such as total surface area as well as the catalyst mass distribution along the surface of plate. As the coating process might alter catalyst properties due to the addition of binder and solvent, the surfaces areas of the fresh OMA-15Ni catalyst and the catalyst slurry used for the washcoating were analyzed. Nitrogen adsorption/desorption measurement of the fresh catalyst and dried catalyst slurry exhibited type-IV isotherms indicating uniform cylindrical mesoporous structure (not shown), with BET total surface areas of 242 and 236 $\text{m}^2 \cdot \text{g}_{\text{cat}}^{-1}$ ($\pm 5 \text{ m}^2 \cdot \text{g}_{\text{cat}}^{-1}$), respectively. The average pore diameters were 10.0 and 9.6 nm for fresh and dried catalyst slurry, calculated using Barrett-Joyner-Halenda (BJH) method. The H_2 -uptake were 142 and 115 $\mu\text{mol g}^{-1}$ for fresh and dried catalyst slurry, and the metal dispersion were 11.1 and 9.2% ($\pm 1.1\%$ absolute). The results indicate that the catalyst slurry preparation had a little influence on the total surface area, but reduced the H_2 -uptake and thus metal dispersion by around 20% relative. It seems that the dissolved binder might partially cover some active sites in porous catalyst structure or influence the reduction of the nickel oxide. Upon mixing with deionized water, the binder (Disperal P2) with an initial particle size of $<20 \mu\text{m}$ disaggregated to less than $<20 \text{ nm}$. Detailed analysis of the fresh catalyst are reported by Aljishi et al. [20].

The catalyst was coated onto a FeCrA-loy plate ($100 \times 40 \text{ mm}$), which was placed at the bottom of the reactor (more details in Section 3). As shown in Figure 1A, the first 35 and last 10 mm of the plate were not coated, in order to allow for formation of a laminar velocity profile and to avoid turbulences caused by the gas inlet and outlet (confirmed by computational fluid dynamics (CFD) modeling, not shown). The coated area was $55 \times 40 \text{ mm}$, with a total catalyst loading of 93 mg. The picture on the left shows a thin layer of catalyst deposited onto the plate with a good coverage over the whole coated area. The SEM picture on the right depicts a clear contrast between the uncoated and catalyst coated regions (Figure 1B) with irregular formed catalyst particles, but no visible indication of binder (Disperal P2) particles originated from the slurry. Figure 1B also indicates overlapping catalyst particles, necessitating the measurement of the coating height profile. The height profile $h(x)$ along the centerline (dashed line in Figure 1A) of the coating was measured, which depended on catalyst size and particle overlap. In the first 20 mm of the coating, the thickness fluctuated between 30–50 μm , then from 20–45 mm the thickness was around 40–80 μm , and at the end of the coating the thickness reached 100 μm (Figure 2A). Considering that the catalyst particles size used for coating were in the range of 20–45 μm , the profilometry and SEM results showed that two or more catalyst were on top of each other. This catalyst accumulation was most likely due to the surface tension close to the frame walls, where the liquid slurry developed a concave liquid surface.

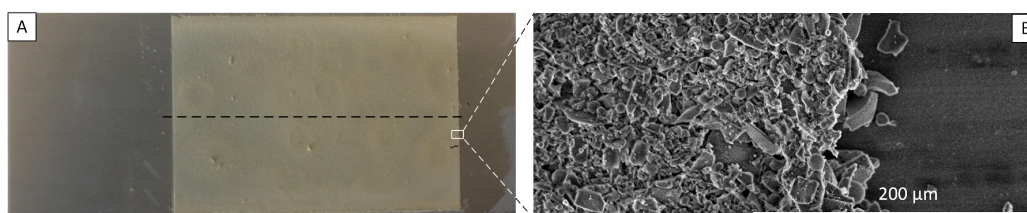


Figure 1. (A) Picture of a catalyst coated FeCrAl-loy plate (100 × 40 mm) and (B) SEM image of the coated and uncoated areas of the plate.

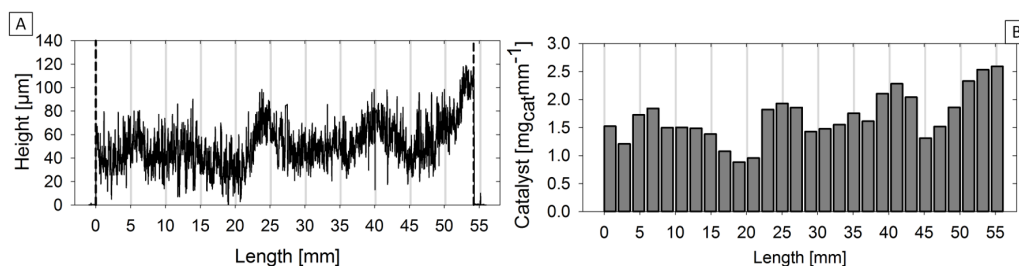


Figure 2. Catalyst coated FeCrAl-loy plate (A) Coating height profile and (B) catalyst mass distribution.

By measuring the catalyst height profile along the coated area of the metal plate, the catalyst mass in the given interval, and the catalyst mass distribution ω_{cat} were calculated as follows:

$$\omega_{cat,\Delta x_i} = \frac{m_{\Delta x_i}}{\Delta x_i} = \frac{h(x_i)}{\int_{x_i}^{x_c} h(x) dx} \cdot m_{cat} \quad (3)$$

In Equation (3), $m_{\Delta x_i}$ represents the catalyst mass in interval i measured in mg_{cat} , Δx_i denotes the interval width (the distance between two capillary positions), m_{cat} the total mass of the catalyst coated on the plate and $h(x_i)$ the average measured height of the interval i . The catalyst mass distribution varied between 1.0 and 2.5 $\text{mg}_{cat} \cdot \text{mm}^{-1}$ (Figure 2B). This is a significant improvement compared to the coating presented in [10], thus hot spots are less probable to occur. The catalyst mass distribution is essential for the development of the reactor model to estimate the kinetic parameters.

2.2. Intra Channel Temperature Gradient

Since a quartz glass was used for optical accessibility, the reactor was not well insulated at the top. Radiation and free convection losses lead to a temperature decrease from the catalyst surface to the quartz glass. This section explains the counter-measures taken to minimize the heat losses and temperature difference long the channel height (i.e., between the catalyst surface and the lower side of the quartz glass).

Figure 3A and B illustrates the configuration with one installed quartz glass and the temperature difference, respectively. For a surface temperature of 325 °C, the lower side of the quartz glass was already 15 °C less. At higher surface temperatures (470 °C) the temperature difference increased to 25 °C. A previous version of the catalytic plate reactor exhibited even larger temperature differences (up to 120 °C) within in a channel height of 5 mm [10]. A high temperature gradient affects the gas diffusion coefficient, the laminar velocity profile and thus the concentration profile along the channel height. The effect of a huge temperature difference on the velocity and concentration profiles is depicted in Figure 3A. Here, the concentration profile of a product “B” might exhibit a minimum, whereas the concentration profile for a reactant “A” might be enhanced. Moreover, the maximum of the laminar velocity profile is shifted towards the lower temperature. Kinetic parameter estimation requires a reactor model that takes all these effects into account. However, by avoiding such a large temperature difference, the reactor model could be significantly simplified (2D versus 1D model).

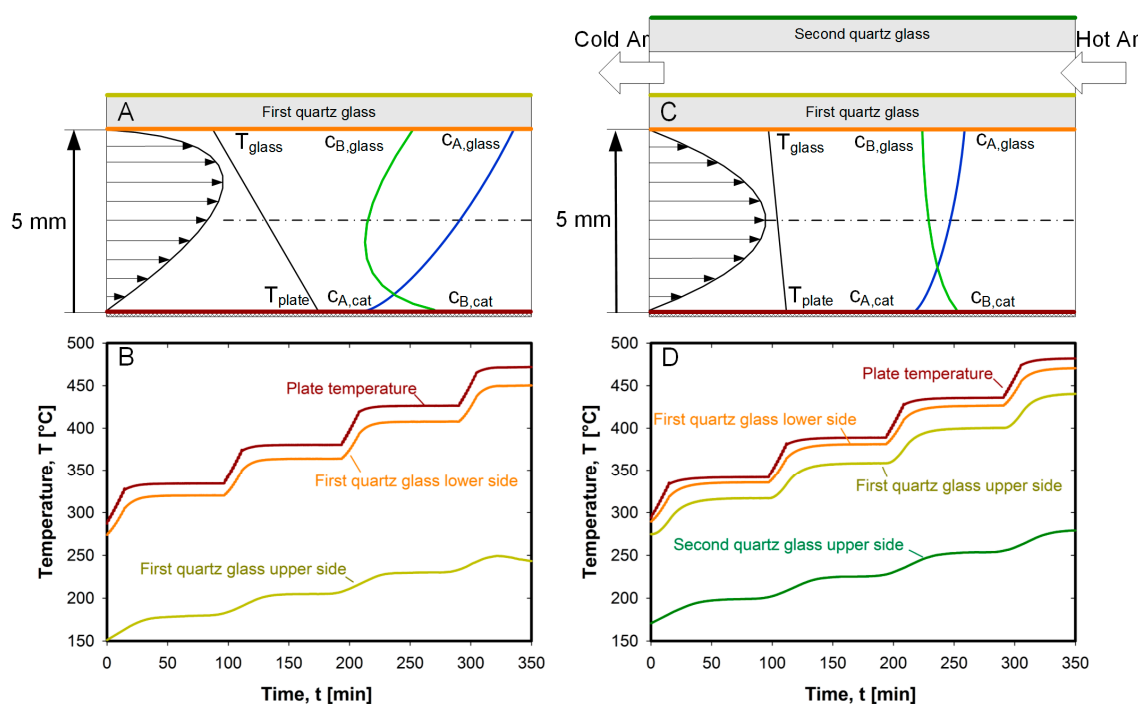


Figure 3. (A) Schematics of velocity and concentration profile of reactant A and product B along the channel height without additional heating; (B) Temperature of plate, lower and upper side of quartz glass without additional heating; (C) Schematics of velocity and concentration profile of reactant A and product B along the channel height with additional heating and (D) Temperature of plate, lower side and upper sides of quartz glasses with additional channel and heating.

To minimize the temperature gradients, a second channel (5 mm height) was designed in which Ar at reaction temperature and at a flow rate of $300 \text{ ml}_N \text{ min}^{-1}$ was fed counter-currently (Figure 3C). The second channel was closed on top by a second quartz glass maintaining optical accessibility for the IR thermography. Temperature gradients of less than 10°C were achieved, for surface temperatures up to 480°C (Figure 3D). As a result, the velocity and concentration profiles were not affected as depicted in Figure 3C. Thus, a simple 1D reactor model can be used to determine the kinetic parameters.

2.3. IR Thermography

IR thermography has been used in several studies to determine the catalyst surface temperature as outlined above. However, to the best of the author's knowledge, the influence of gaseous species in the IR emissions has not been yet investigated. In the present work a SWIR camera was used, and this section discusses three aspects (1) whether or not polyatomic (i.e., IR absorbing) molecules influence the temperature measurement; (2) camera calibration and (3) the results for the CO_2 methanation.

Figure 4A depicts a 2D heat map of an uncoated FeCrAl-loy plate. In addition, the flow straightener and four thermocouples are visible, which were used to determine the temperature differences as discussed in Section 2.2 (Figure 3C,D). Figure 4B shows the results of IR emissions measured along the dashed line (Figure 4A) for four different gas compositions representing catalyst reduction and CO_2 methanation with and without product formation. In detail, the first IR profile was measured with 50 mol% H_2 and 50 mol% Ar. Since H_2O is produced during catalyst reduction, the second profile was measured with 40 mol% H_2 , 40 mol% Ar and 10 mol% H_2O . The third profile with 50 mol% H_2 , 10 mol% CO_2 , and 40 mol% Ar refers to the inlet condition used for the CO_2 methanation test. Profile 4 was measured with a gas mixture of 28 mol% H_2 , 6 mol% CO_2 , 5 mol% CH_4 , 11 mol% H_2O and 50 mol% Ar, representing the reaction products for the CO_2 methanation with a conversion of 53%.

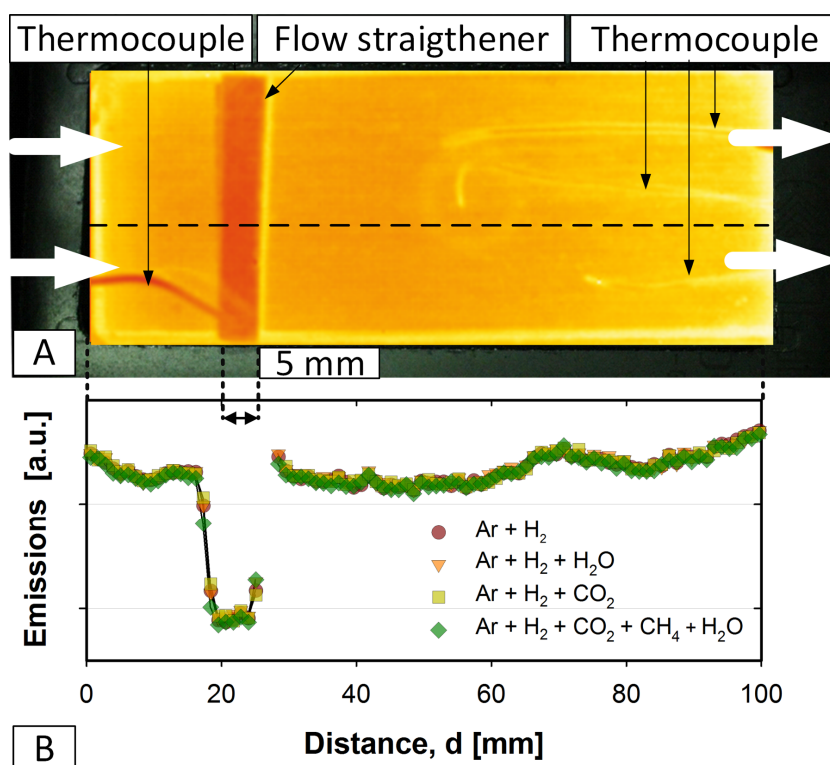


Figure 4. (A) The 2D infrared (IR) picture of an uncoated FeCrAl-loy plate; (B) IR emissions measured along the dashed line on an uncoated plate for four different gas compositions: (1) ● H₂ and Ar, (2) ▼ H₂, Ar and H₂O, (3) ■ H₂, CO₂, and Ar, (4) ◆ H₂, CO₂, CH₄, H₂O and Ar.

The emissions profiles recorded for the different gas mixtures overlapped each other perfectly (Figure 4B), confirming that CO₂ and products H₂O and CH₄ did not adsorb the emitted infrared emissions in the short wavelength, and thus did not influence in the surface temperature measurement.

The calibration curves for the coated and uncoated areas of the plate are depicted in Figure 5A and B, respectively. The data were fitted to a cubic polynomial with four parameters.

$$T = A + B \cdot I + C \cdot I^2 + D \cdot I^3 \quad (4)$$

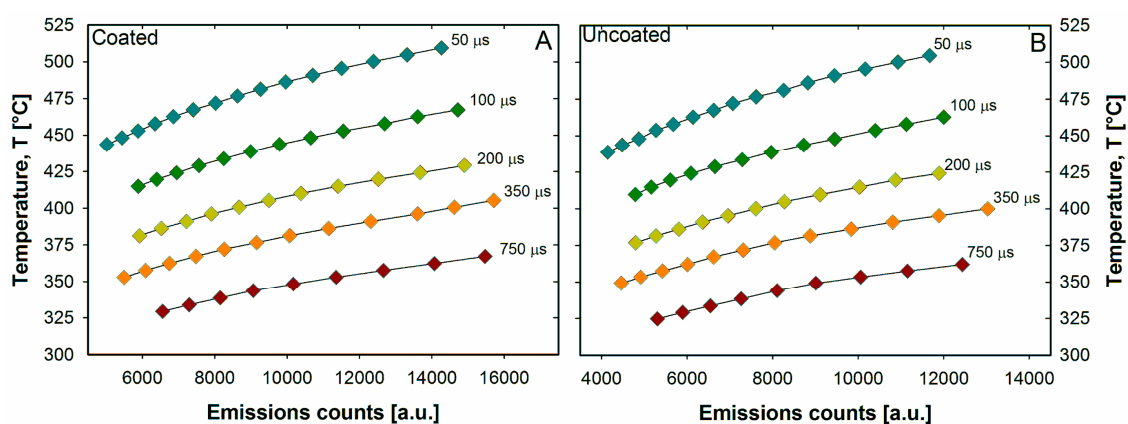


Figure 5. IR calibration curves at different integration times, ◆ 750 μs, ◆ 350 μs, ◆ 200 μs, ◆ 100 μs and ◆ 50 μs for: (A) Catalyst coated area and (B) uncoated area of the FeCrAl-loy plate.

In Equation (4), T represents the calculated surface temperature, I denotes the intensity measured at the corresponding integration time, and A , B , C , and D are the estimated coefficients (Table 1).

Table 1. Coefficients of Equation (4) for the IR calibration for the catalyst coated and uncoated areas, determined at different integration times in the temperature range of 325–500 °C.

	Integration Time, μs	A	B	C	D
Coated area	750	262.88	0.015	-8.05×10^{-7}	1.92×10^{-11}
	350	285.40	0.017	-1.01×10^{-6}	2.63×10^{-11}
	200	311.62	0.016	-8.08×10^{-7}	1.80×10^{-11}
	100	333.27	0.019	-1.09×10^{-6}	2.66×10^{-11}
	50	368.11	0.019	-9.72×10^{-7}	2.15×10^{-11}
Uncoated area	750	265.15	0.016	-1.02×10^{-6}	2.68×10^{-11}
	350	290.80	0.018	-1.13×10^{-6}	3.02×10^{-11}
	200	308.09	0.021	-1.34×10^{-6}	3.74×10^{-11}
	100	322.18	0.028	-2.23×10^{-6}	7.33×10^{-11}
	50	369.11	0.023	-1.36×10^{-6}	3.59×10^{-11}

With the calibration curve, the temperature of the whole catalyst surface with a high temporal and spatial resolution can be determined. This is a significant advantage compared to pyrometers and thermocouples that measure a single spot temperature only. Figure 6A,B visualizes a 2D and 3D surface temperature plot obtained during the CO_2 methanation at 425 °C with an inlet flow rate of 150 $\text{ml}_\text{N} \text{min}^{-1}$ and a gas mixture of 67 mol% H_2 , 13 mol% CO_2 and 20 mol% Ar. The brighter the spot the higher is the intensity of the emissions and thus the temperature on the surface.

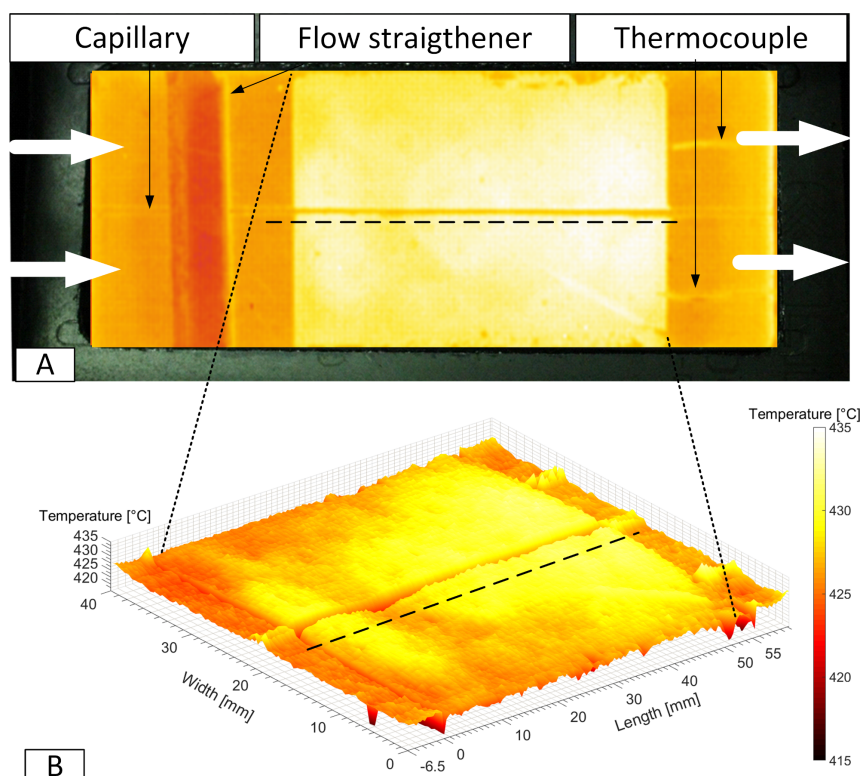


Figure 6. (A) Qualitative 2D IR emission and (B) quantitative 3D surface temperatures obtained during the CO_2 methanation at a temperature of 425 °C with an inlet flow rate of 150 $\text{ml}_\text{N} \text{min}^{-1}$ (67 mol% H_2 , 13 mol% CO_2 and 20 mol% Ar). Camera integration time 100 μs .

Figure 6A depicts the movable sampling capillary in the middle of the reactor as well as the flow straightener and two thermocouples used for IR calibration. The dashed line indicates the position where the temperature line profile was acquired, which is shown in Figure 7. Figure 6B illustrates nicely, a 3D surface temperature plot of the catalyst coated area, which also provides qualitative information about the catalyst mass distribution. In detail, the brighter area, i.e., higher surface temperature, indicates a higher catalyst loading, which coincides with the profilometry data (see Figure 2). IR thermography confirms that the catalyst coating process ought to be optimized to obtain a homogenous catalyst mass distribution along the width and length of plate.

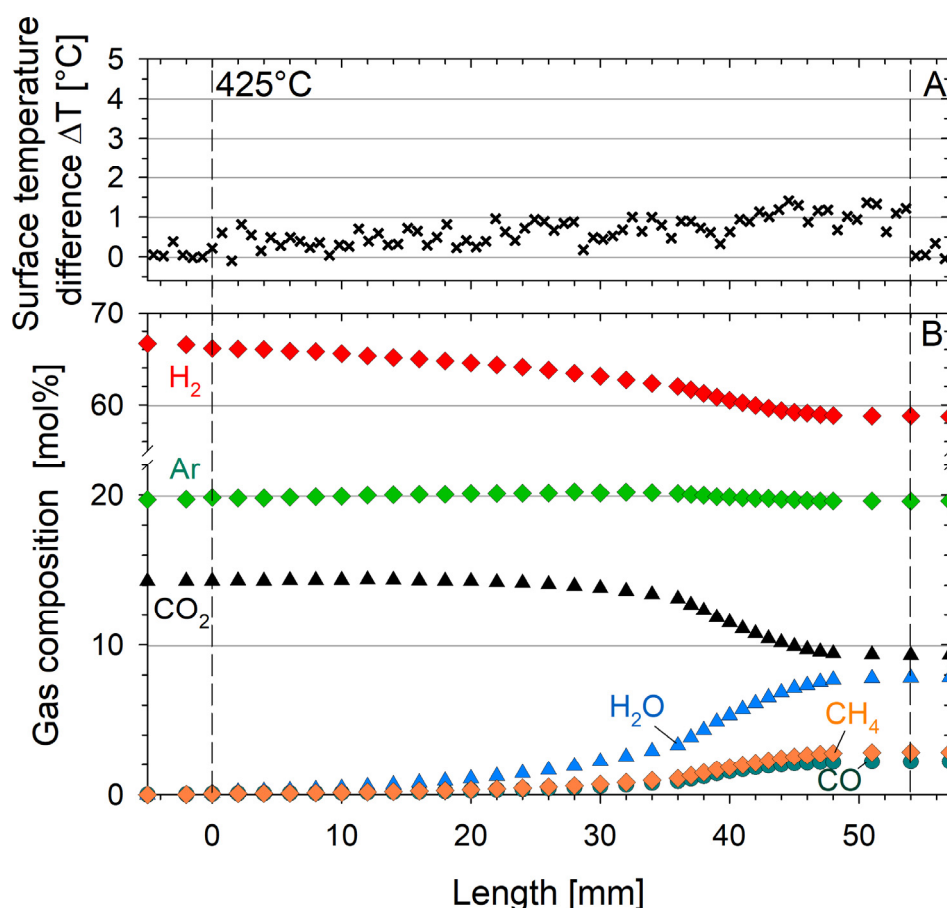


Figure 7. Results for coated plate with OMA-15Ni catalyst for $H_2/CO_2 = 5$, 1 bar: (A) Catalyst surface temperature difference and; (B) Measured axial gas composition profiles. The dashed lines indicate the beginning and the end of the coated area.

2.4. CO₂ Methanation Activity

Figure 7A,B illustrates temperature difference line profile and gas composition profile for the CO₂ methanation test conducted at 425 °C with a total flow rate of 150 ml_N min⁻¹ (67 mol% H₂, 13 mol% CO₂ and 20 mol% Ar). The coating starts at 0 mm and ends at 55 mm. The surface temperature along the center line was around 425 and 430 °C. The upper part of the diagram (Figure 7A) illustrates the temperature difference before and after adding CO₂, measured along the catalyst plate, dashed line in Figure 6B. The temperature profile indicates an almost constant temperature distribution. The temperature difference before the coating start was negligible and increased slightly towards the end of the coated area. After 35 mm, the temperature difference reached 1 °C, thereafter it remains almost constant until the end of the coated area. Figure 7B shows the axial gas composition after

adding CO₂. The total C, H and O balance was within $\pm 5\%$. In total, more than 30 high quality data points per gas species were collected with 1 experiment.

The gas composition did not change before the coating begins. Thereafter, H₂ and CO₂ decreased from 67 to 59 mol% and from 13 to 9.3 mol%, respectively towards the end of the plate. While CH₄ and H₂O increased to 2.9 and 7.8 mol%, respectively. Besides CH₄, a considerable amount of CO was formed (2.2 mol% at the end of the plate). The increase in the CO concentration can be explained due to the reversed water gas shift ($\text{CO}_2 + \text{H}_2 \leftrightarrow \text{CO} + \text{H}_2\text{O}$), which also lead to an increase in the H₂O content. The conversion of CO₂ was 34% and the selectivities towards CH₄ and CO were 60% and 40%, respectively. The atomic carbon, hydrogen and oxygen balances for this experiment was within $100 \pm 3\%$.

3. Materials and Methods

3.1. Setup and Reactor

The simplified P&ID of the setup is depicted in Figure 8; it consists of a gas mixing station, water saturator, optically accessible channel reactor, infrared camera, movable sampling system and gas analyzer. All gases (i.e., Ar, H₂, CO₂, CH₄) were fed through calibrated mass flow controllers (red-smart Vögtlin, Aesch, Switzerland), mixed and preheated before entering the reactor. The water content in the gas mixture could be adjusted by means of a calibrated saturator. The total pressure was controlled by a backpressure regulator (Equilibar LF, Fletcher, NC, USA). The product gas was cooled to condense out the water and then sent to the fume hood.

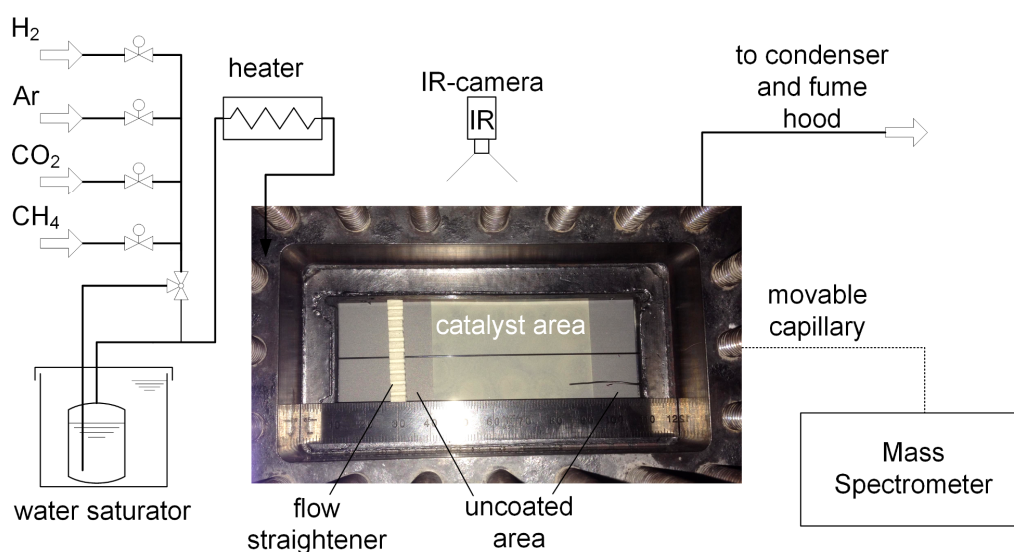


Figure 8. Scheme of the catalytic plate reactor test rig.

A schematic side view of the catalytic plate reactor (CPR) is shown in Figure 9A. It is a further development of the reactor described in [10]. The reactor was machined from stainless steel SS-316L with effective channel dimensions of $40 \times 100 \times 5$ mm and three inlet and outlet ports with diameter of 2 mm each. At the bottom of the channel a catalyst coated plate was placed, Section 3.2, while the top was closed with a set of two clear fused quartz glass plates, installed for optically accessibility and minimization of intra-channel temperature gradient, Section 3.3. The fused quartz glass plates (Heraeus, TSC-3, Hanau, Germany) had a 90% transmissivity in the 0.2–2.0 μm wavelength range [21], enabling the usage of a shortwave infrared camera (FLIR, SC2500, Burlington, ON, Canada) [22] to determine the catalyst surface, Section 3.4. The reactor itself was heated by a set of 6 heating cartridges evenly distributed under the plate to assure homogeneous heating. The reactor was completely

insulated leaving only the glass exposed. High temperature gaskets (Klinger PMS-AS, Bradford, UK) were used between the quartz glass and stainless-steel part. The gaskets had a thickness of 1.6 mm with a compressibility factor of 30%. The reactor was pressure tested up to 10 bar_{abs} at 600 °C. The reactor was equipped with a thin (O.D. 0.5 mm, SS-316L) movable sampling capillary to quantify the axial gas species composition profiles with a high spatial resolution (0.1 mm) above the catalyst. The capillary was installed along the whole channel length (i.e., supported on two points), it was sealed at one of its ends, but it contained a laser drilled sampling orifice with diameter of 250 μm facing the catalyst surface (Figure 9B and C). By doing this, downwards bending of the capillary could be avoided, which has been a main disadvantage of the setup that introduced an open ended capillary half way inside the channel reactor [10].

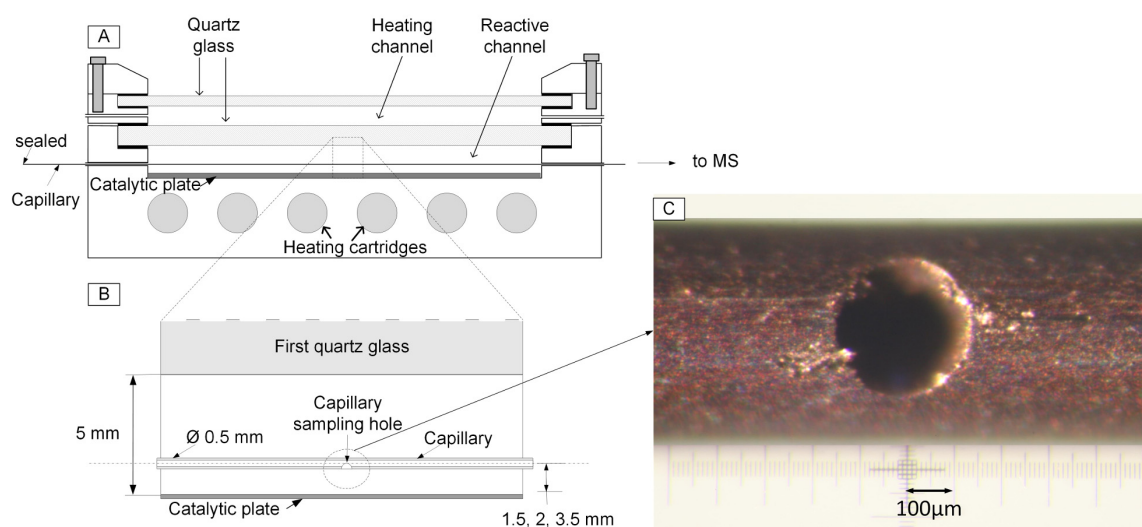


Figure 9. (A) Schematic side view of the catalytic plate reactor body with a set of 6 heating cartridges and a set of two quartz glasses for optical accessibility (not to scale); (B) Detailed area of the reactor channel with the capillary going through; (C) Picture of the capillary with the sampling orifice.

Furthermore, in our new and optimized reactor design, the height of the capillary above the catalyst can be adjusted from 1.0 to 3.5 mm to obtain quasi-radial concentration profiles, thus determining an accurate average gas composition as shown schematically in Figure 9B. The capillary was moved using a LabVIEW controlled linear stage (PBC linear, Rockford, IL, USA) and connected to a calibrated mass spectrometer (Hiden Analytical HPR-20, Warrington, UK) for online gas analysis. The sample flow rate through the capillary was set to 1 mL min⁻¹, which was less than 1% of the total flow rate used in the activity experiment. A piece of cordierite monolith (5 × 5 × 40 mm) with 64 channels per square inch was installed before the coated area that served as a flow straightener and diminished the vortices that might have been formed at the channel inlet ports (Figure 8).

3.2. Catalyst Coating and Catalyst Mass Distribution

Ordered mesoporous nickel-alumina (OMA-15Ni) catalyst was synthesized following the evaporation induced self-assembly method used by Aljishi et al. [20]. In detail, 1 g of triblock copolymer (Pluronic® P-123, Sigma Aldrich, Oakville, ON, Canada) was dissolved in 20 mL anhydrous ethanol until a homogeneous solution was obtained. Subsequently 3.22 g aluminum-isopropoxide (≥98%, Sigma Aldrich, Oakville, ON, Canada) and 0.75 g of nickel (II) nitrate hexahydrate (≥98.5%, Sigma Aldrich, Oakville, ON, Canada) were added to achieve the desired catalyst mass and nickel target loadings. Nitric acid (68 wt%, Fisher Scientific, Ottawa, ON, Canada) was added to provide the acidic environment to enhance mesoporous formation. The solution was stirred for 5 h at 600 rpm at room temperature. The homogenized solution obtained, was dried at 60 °C for 48 h and subsequently

calcined in a muffle furnace with heating rate of $1\text{ }^{\circ}\text{C min}^{-1}$ for 5 h at the targeted calcination temperature, $500\text{ }^{\circ}\text{C}$. The fresh catalyst contained 15 wt% of Ni. The catalyst was sieved and the particle size of $20\text{--}45\text{ }\mu\text{m}$ was used for coating onto a metal FeCrAl-loy plate. Prior to the coating the FeCrAl-loy plate ($100 \times 40\text{ mm}$) was calcined at $1000\text{ }^{\circ}\text{C}$ for 36 h to assure the growth of alumina whiskers (confirmed by XRD analysis, not shown). The heat-treated plate was weighed then taped leaving an area of $55 \times 40\text{ mm}$ exposed for the coating.

A water-isopropanol slurry containing the catalyst and an alumina based binder was prepared. The binder (Disperal P2, Sasol, Hamburg, Germany) was added to DI water and stirred at $25\text{ }^{\circ}\text{C}$ for 60 min. Upon stirring the binder particles of $<20\text{ }\mu\text{m}$ disperse to aggregates of around 20 nm. The binder was used to improve the adherence of the catalyst to the metal plate. Then, isopropanol and catalyst was added and stirred at $25\text{ }^{\circ}\text{C}$ for 60 min. The slurry was kept under stirring until coating onto the plate. The water to isopropanol volume ratio for solvent preparation was $1:4\text{ ml}_w/\text{ml}_{iso}$. The catalyst to binder weight ratio was $9:1\text{ g}_{cat}/\text{g}_{binder}$. The total solid (catalyst and binder) to liquid ratio for the slurry preparation was $0.25:5\text{ g}_{solid}/\text{ml}_{solution}$.

A polylactic acid (PLA) rectangular frame (inner dimensions of $55 \times 40\text{ mm}$) produced by 3D printing was fixed on top of the heat-treated FeCrAl-loy plate. Then, 1.3 mL of slurry was poured into the framed area using a glass pipette. Once the slurry covered the entire coating area, the plate was air dried overnight and subsequently calcined at $375\text{ }^{\circ}\text{C}$ for 5 h. The weight of the dried and calcined plate was recorded to calculate the actual total catalyst loading.

The adherence of the catalyst coating was verified via mechanical tests in a flow channel with a flow rate of up to $400\text{ ml}_N\text{ min}^{-1}$. No catalyst loss nor damage to the coating was observed (not shown).

To investigate the influence of the binder and solvent on the catalyst properties, the dried slurry was calcined at the same temperature (i.e., $375\text{ }^{\circ}\text{C}$ for 5 h). Fresh catalyst and calcined slurry were then analyzed by nitrogen adsorption/desorption and hydrogen uptake (Autosorb iQ, Quantachrome, Boynton Beach, FL, USA). Nitrogen adsorption/desorption measurements ($-196\text{ }^{\circ}\text{C}$) were conducted to determine total surface area. Before the analysis, the sample was degassed under vacuum for 12 h at $200\text{ }^{\circ}\text{C}$. For hydrogen uptake (chemisorption), approximately 100 mg of the sample was placed in a U-shaped quartz tube, preheated in He at $120\text{ }^{\circ}\text{C}$ with a heating rate of $20\text{ }^{\circ}\text{C min}^{-1}$ for 1 h, then reduced with H_2 at its optimum reduction temperature obtained from catalyst H_2 -TPR [20] for another 3 h, then evacuated for 1 h and subsequently cooled to $40\text{ }^{\circ}\text{C}$, where all measurements were taken at pressures ranging from 50 to 800 mbar. All surface area analyzes were conducted 3 time to assure data accuracy and reproducibility.

Scanning Electron Microscopy (SEM) analysis were performed using a field emission scanning electron microscope (FEI Inspect F-50, Hillsboro, OR, USA) to examine the morphology of coating.

The coating height profile was measured after performing the activity measurement and kinetic data acquisition by means profilometry (Dektak XT, Bruker, Tucson, AZ, USA). The vertical measurement limit for profilometry was 1 mm, and the horizontal span in a single acquisition was 55 mm. The stylus had a diameter of $12.5\text{ }\mu\text{m}$ and the force applied for the profilometry test was set to be 1 mg. The profilometer resolution allowed collecting 55,000 data points in each profile of 55 mm total length (1 data point per μm length).

3.3. Intrachannel Temperature Gradient Minimization

Temperatures difference across the channel height were examined for two scenarios. In the first case, only one quartz glass was installed in the reactor enclosing a first channel (reactor channel) where an uncoated plate was placed. In the second case, a second quartz glass was installed on top the first quartz glass, thus it enclosed a second channel (heating channel).

In the first scenario, three surface temperatures were measured as a function of the time using K-type thermocouples: plate surface, lower side and upper side of the first quartz glass. In the second scenario, four surface temperatures were measured as a function of the time using K-type

thermocouples: plate surface, lower side and upper side of the first quartz glass, and upper side of the second quartz glass, Figure 3.

The temperature range of 325–500 °C was chosen based on thermodynamic considerations and reactivity measurements reported elsewhere for CO₂ methanation over supported alumina and ordered mesoporous Ni/Al₂O₃ [20]. A heat-treated but uncoated plate was installed in the reactor. The channel reactor was fed with constant Ar flowrate of 100 ml_N min⁻¹, while it was heated with a rate of 5 °C min⁻¹ to its target temperature, where it was hold for about 80 min to reach thermal steady state.

3.4. IR Thermography for Catalyst Surface Temperature

The intensity of the infrared radiation emitted by the hot surface was quantified by an infrared camera, (FLIR, SC2500, Burlington, ON, Canada) working in the short wavelength (0.9–1.7 μm) region [22]. The camera was equipped with an indium gallium arsenide (InGaAs) sensor with 320 × 256 pixels, translating into a high spatial resolution of 3 emission data points per mm length (or 9 data points per 1 mm² surface).

To study the influence of polyatomic (IR adsorbing) molecules on the surface temperature measurement, a heat-treated but uncoated plate was installed in the channel reactor. The reactor was then heated to its target temperature (350 °C) at a rate of 5 °C min⁻¹ under 100 ml_N min⁻¹ of Ar. Four different gas compositions representing catalyst reduction and CO₂ methanation with and without product formation were used: (1) 50 mol% H₂ and 50 mol% Ar, (2) 40 mol% H₂, 40 mol% Ar and 10 mol% H₂O, (3) 50 mol% H₂, 10 mol% CO₂, and 40 mol% Ar, and (4) 28 mol% H₂, 6 mol% CO₂, 5 mol% CH₄, 11 mol% H₂O and 50 mol% Ar. For each gas composition, a 2D infrared surface and a line profile were recorded.

Next, the infrared camera was calibrated for the catalyst coated and uncoated area on the FeCrAl-loy plate. Since the catalyst color changed from green to black during the catalyst reduction, the calibration was done after reduction. The reactor was heated stepwise under a constant flow of 50 mol% of H₂ and 50 mol% of Ar, while the corresponding IR intensity at spots (3 × 3 pixel) close to each installed surface thermocouple was acquired. Due to the broad temperature range, 325–500 °C, five different integration times (equivalent to camera shutter time) were used to measure the intensity (750 to 35 μs). At higher temperatures and thus higher radiation energy and the integration time was reduced to avoid saturation of the InGaAs detector.

3.5. Spatially-Resolved Concentration and Temperature During CO₂ Methanation

Prior to the experiments, the catalysts were reduced with 50 mol% H₂ in Ar for 8 h at the respective reduction temperature (580 °C) determined via H₂-TPR [20]. After the reduction, the reactor was cooled to 425 °C, the reaction temperature used in this study. Then, the sampling orifice of the capillary was moved to the zero position, approx. 6 mm before the coated area starts. H₂ (99.999% Megs, Montreal, Canada) and Ar (99.999% Megs, Montreal, QC, Canada) flow rates were set to 100 and 30 ml_N min⁻¹, respectively, and the first IR surface and line profile were recorded. Then CO₂ (99.995%, Megs, Montreal, QC, Canada) was fed stepwise until the desired volumetric flow rate of 150 ml_N min⁻¹ was reached. The reaction was performed at 1.5 bar_{abs} with H₂/CO₂ ratio of 5:1. The experiments were conducted under laminar flow conditions. Thus, the mass transfer perpendicular to the flow direction was clearly defined by diffusion.

The sampling capillary started to move after the concentration at the zero position had reached a steady-state value. At this time, a second IR surface and line profile were recorded. While sampling, the capillary was held for 120 s at each position and moved in flow direction to the end of the reactor. For this study, the experimental run consisted of 35 capillary positions along the channel reactor.

The sampling gas flow rate was set to 1 ml_N min⁻¹ (<1% of the total flow rate) and heated to 180 °C to avoid condensation of water inside of the capillary. The gas composition was measured online via calibrated quadrupole mass spectrometer (Hiden Analytical HPR-20, Warrington, UK). Before the test, the mass spectrometer was specifically calibrated for H₂ (2 amu), CH₄ (15 amu), H₂O

(18 amu), CO (28 amu), Ar (40 amu) and CO₂ (44 amu). The contribution of the fragmentation of CO₂ to the CO signal at mass 28 was taken into account in the calibration. Argon was set as an internal standard.

4. Conclusions

An optimized optically accessible channel reactor with spatially-resolved measurement techniques was designed that allows to collect a significantly larger set of kinetic data for the parameter estimation than by use of typical steady-state reactors with concentration measurements at the outlet only. In detail, a small movable sampling capillary and a shortwave infrared camera enabled simultaneous measurement of the gas composition and catalyst surface temperature along the reactor axis. Additional advantages of the new setups are:

- Temperature gradient across the reactive channel height was reduced to less than 10 K. Thus, laminar velocity and radial concentration profiles were not deformed.
- SWIR camera is ideal to determine the catalyst surface temperature under operating conditions. It even allows to qualitatively determine the catalyst mass distribution of coating.
- Polyatomic molecules did not influence the temperature measurements.
- Spatially-resolved catalyst mass distribution can be determined by profilometry.

It can be summarized that the developed catalytic plate reactor with spatially-resolved measurements is very suitable to study the kinetic of highly exothermic, fast and heterogeneously catalyzed reactions such as CO₂ methanation.

Acknowledgments: The authors acknowledge the financial support from the Natural Sciences and Engineering Research Council of Canada (NSERC, RGPIN/04685-2014).

Author Contributions: Jan Kopyscinski and Jose A. Hernandez Lalinde conceived and designed the experiments; Jose A. Hernandez Lalinde design the reactor and performed the experiments; Jose A. Hernandez Lalinde, Kevin Kofler and Xuejie Huang analyzed the data; Kevin Kofler and Xuejie Huang contributed reagents/materials/analysis tools; Jose A. Hernandez Lalinde and Jan Kopyscinski wrote the paper.

Conflicts of Interest: The authors declare no conflict of interest.

References

1. Kopyscinski, J.; Schildhauer, T.J.; Biollaz, S.M.A. Fluidized-Bed Methanation: Interaction between Kinetics and Mass Transfer. *Ind. Eng. Chem. Res.* **2011**, *50*, 2781–2790. [[CrossRef](#)]
2. Diehm, C.; Karadeniz, H.; Karakaya, C.; Hettel, M.; Deutschmann, O. Chapter Two—Spatial Resolution of Species and Temperature Profiles in Catalytic Reactors: In Situ Sampling Techniques and CFD Modeling. In *Advances in Chemical Engineering*; Dixon, A.G., Ed.; Modeling and Simulation of Heterogeneous Catalytic Processes; Academic Press: Cambridge, MA, USA, 2014; Volume 45, pp. 41–95.
3. Sa, J.; Fernandes, D.L.A.; Aiouache, F.; Goguet, A.; Hardacre, C.; Lundie, D.; Naeem, W.; Partridge, W.P.; Stere, C. SpaciMS: spatial and temporal operando resolution of reactions within catalytic monoliths. *Analyst* **2010**, *135*, 2260–2272. [[CrossRef](#)] [[PubMed](#)]
4. Choi, J.-S.; Partridge, W.P.; Pihl, J.A.; Kim, M.-Y.; Kočí, P.; Daw, C.S. Spatiotemporal distribution of NO_x storage and impact on NH₃ and N₂O selectivities during lean/rich cycling of a Ba-based lean NO_x trap catalyst. *Catal. Today* **2012**, *184*, 20–26. [[CrossRef](#)]
5. Choi, J.-S.; Partridge, W.P.; Daw, C.S. Spatially resolved in situ measurements of transient species breakthrough during cyclic, low-temperature regeneration of a monolithic Pt/K/Al₂O₃ NO_x storage-reduction catalyst. *Appl. Catal. A* **2005**, *293*, 24–40. [[CrossRef](#)]
6. Horn, R.; Degenstein, N.J.; Williams, K.A.; Schmidt, L.D. Spatial and temporal profiles in millisecond partial oxidation processes. *Catal. Lett.* **2006**, *110*, 169–178. [[CrossRef](#)]
7. Horn, R.; Williams, K.A.; Degenstein, N.J.; Bitsch-Larsen, A.; Dalle Nogare, D.; Tupy, S.A.; Schmidt, L.D. Methane catalytic partial oxidation on autothermal Rh and Pt foam catalysts: Oxidation and reforming zones, transport effects, and approach to thermodynamic equilibrium. *J. Catal.* **2007**, *249*, 380–393. [[CrossRef](#)]

8. Horn, R.; Williams, K.A.; Degenstein, N.J.; Schmidt, L.D. Mechanism of H₂ and CO formation in the catalytic partial oxidation of CH₄ on Rh probed by steady-state spatial profiles and spatially resolved transients. *Chem. Eng. Sci.* **2007**, *62*, 1298–1307. [[CrossRef](#)]
9. Weber, D.; Holland, D.J.; Gladden, L.F. Spatially and chemically resolved measurement of intra- and inter-particle molecular diffusion in a fixed-bed reactor. *Appl. Catal. Gen.* **2011**, *392*, 192–198. [[CrossRef](#)]
10. Kopyscinski, J.; Schildhauer, T.J.; Vogel, F.; Biollaz, S.M.A.; Wokaun, A. Applying spatially resolved concentration and temperature measurements in a catalytic plate reactor for the kinetic study of CO methanation. *J. Catal.* **2010**, *271*, 262–279. [[CrossRef](#)]
11. Bosco, M.; Vogel, F. Optically accessible channel reactor for the kinetic investigation of hydrocarbon reforming reactions. *Catal. Today* **2006**, *116*, 348–353. [[CrossRef](#)]
12. Shakir, O.; Yezerets, A.; Currier, N.W.; Epling, W.S. Spatially resolving concentration and temperature gradients during the oxidation of propylene on Pt/Al₂O₃. *Appl. Catal. Gen.* **2009**, *365*, 301–308. [[CrossRef](#)]
13. Frey, M.; Romero, T.; Roger, A.C.; Edouard, D. Open cell foam catalysts for CO₂ methanation: Presentation of coating procedures and in situ exothermicity reaction study by infrared thermography. *Catal. Today* **2016**. [[CrossRef](#)]
14. Schüler, C.; Hinrichsen, O. Entwicklung eines optisch zugänglichen Reaktors zur Thermographiemessung in einer Katalysatorschüttung. *Chem. Ing. Tech.* **2016**, *88*, 1693–1702. [[CrossRef](#)]
15. Götz, M.; Lefebvre, J.; Mörs, F.; McDaniel Koch, A.; Graf, F.; Bajohr, S.; Reimert, R.; Kolb, T. Renewable Power-to-Gas: A technological and economic review. *Renew. Energy* **2016**, *85*, 1371–1390. [[CrossRef](#)]
16. Wender, I. Reactions of synthesis gas. *Fuel Process. Technol.* **1996**, *48*, 189–297. [[CrossRef](#)]
17. Weatherbee, G.D.; Bartholomew, C.H. Hydrogenation of CO₂ on group VIII metals: I. Specific activity of NiSiO₂. *J. Catal.* **1981**, *68*, 67–76. [[CrossRef](#)]
18. Chiang, J.H.; Hopper, J.R. Kinetics of the hydrogenation of carbon dioxide over supported nickel. *Ind. Eng. Chem. Prod. Res. Dev.* **1983**, *22*, 225–228. [[CrossRef](#)]
19. Mills, G.A.; Steffgen, F.W. Catalytic Methanation. *Catal. Rev.* **1974**, *8*, 159–210. [[CrossRef](#)]
20. Aljishi, A.; Veilleux, G.; Hernandez Lalinde, J.A.; Kopyscinski, J. The effect of synthesis parameters on ordered mesoporous nickel alumina catalyst for CO₂ methanation. *Appl. Catal. Gen.* **2018**, *549*, 263–272. [[CrossRef](#)]
21. TSC Series. Available online: https://www.heraeus.com/media/media/hqs/doc_hqs/products_and_solutions_8/solids/TSC_Series_EN.pdf (accessed on 11 January 2018).
22. FLIR SC2500 Manual. Available online: [http://support.flir.com/DocDownload/Assets/dl/dc065u\\$e.pdf](http://support.flir.com/DocDownload/Assets/dl/dc065u$e.pdf) (accessed on 19 February 2018).



© 2018 by the authors. Licensee MDPI, Basel, Switzerland. This article is an open access article distributed under the terms and conditions of the Creative Commons Attribution (CC BY) license (<http://creativecommons.org/licenses/by/4.0/>).